Soft Matter

PAPER

View Article Online
View Journal | View Issue

Open Access Article. Published on 09 June 2025. Downloaded on 5/9/2026 5:04:01 AM.
This article is licensed under a Creative Commons Attribution-NonCommercial 3.0 Unported Licence.

Cite this: *Soft Matter*, 2025, **21**, 5529

Brownian dynamics simulation of the diffusion of rod-like nanoparticles in polymeric gels†

Mohammad-Reza Rokhforouz,[a] Don D. Sin,[b] Sarah Hedtrich[cde] and James J. Feng *[af]

Rod-like nanoparticles (RNPs) have been shown to diffuse faster than spherical ones in polymeric hydrogels, but the underlying physics is not well understood. We develop a 3D Brownian dynamics model to investigate this phenomenon, representing the gel as a random network of rigid fibers in water and incorporating both steric repulsion and adhesive interactions. In non-adhesive gels, RNP diffusivity increases monotonically with the aspect ratio while its hydrodynamic diameter is kept constant, in agreement with the predictions of an obstruction scaling (OS) model. However, our model predicts a much higher diffusivity than the OS model, by up to 5 times for higher aspect ratios. To rationalize this discrepancy, we demonstrate that RNPs experience a skewed pore-size distribution in favor of the larger pores; they spend more time in coarser regions of the gel than in denser regions. Moreover, the RNPs execute a meandering motion in the coarser regions with pronounced rotational and transverse diffusion. In contrast, in denser regions, restricted rotation results in predominantly longitudinal diffusion. This anisotropy in diffusion further elevates the translational diffusivity of RNPs. Our model also reveals a competition between the steric and adhesive interactions, where steric repulsion limits access to adhesion sites, and produces a diffusivity intermediate between the purely steric and purely adhesive cases. Overall, our results show an even greater advantage for RNPs, in terms of rapid diffusion in hydrogels, than previously anticipated by using the OS model.

Received 24th February 2025,
Accepted 7th June 2025

DOI: 10.1039/d5sm00195a

rsc.li/soft-matter-journal

1. Introduction

The diffusion of nanoparticles (NPs) in hydrogels (*e.g.*, mucus) is determined not only by their size and surface chemistry, but also by their shape.[1] It is known that the NPs should be smaller than the hydrogel's mesh size and possess a near-neutral charge for effective penetration into the gel.[2] Inspired by the fact that the majority of microbial residents in the gastrointestinal tract are rod-shaped,[3] rod-like NPs (RNPs) have emerged as an alternative to conventional spherical nanoparticles (SNPs). Yu *et al.*[4] showed that 80 × 240 nm RNPs diffuse faster than their 80 nm spherical counterparts in intestinal mucus. Wang *et al.*[5] captured the same trend and also showed that the diffusivity would fall again for overly long rods. Since then, experimental,[6–12] theoretical,[5] and computational[12–16] investigations have been conducted to examine the underlying mechanisms responsible for the superiority of RNPs in penetrating hydrogels.

In the literature, three protocols have been employed to examine the effects of the aspect ratio of RNPs. The d-protocol compares RNPs with the same minor-axis diameter but different lengths.[4] The v-protocol compares RNPs with the same volume,[14] and the hd-protocol compares RNPs with the same hydrodynamic diameter,[5] *i.e.*, the diameter of a sphere possessing the same Stokes–Einstein diffusivity as the RNP in the solvent (see eqn (1) for details).

In non-adhesive gels, with steric repulsion only, our understanding of NP diffusion has come mostly from the obstruction-scaling (OS) model. Essentially, the model assumes that the obstacles reduce the NP diffusivity by a factor that is the probability of the NP encountering a polymer chain. By extending Ogston's OS model[17] and conducting experiments, Wang *et al.*[5] showed that in the d-protocol, longer rods with the same minor-axis diameter exhibit slower diffusion than shorter ones. This is essentially the same trend as that observed for diffusion

---

[a] *Department of Chemical and Biological Engineering, University of British Columbia, Vancouver, British Columbia, Canada. E-mail: james.feng@ubc.ca*
[b] *Centre for Heart Lung Innovation, University of British Columbia, Vancouver, British Columbia, Canada*
[c] *Faculty of Pharmaceutical Sciences, University of British Columbia, Vancouver, British Columbia, Canada*
[d] *School of Biomedical Engineering, University of British Columbia, Vancouver, British Columbia, Canada*
[e] *Center of Biological Design, Berlin Institute of Health at Charité – Universitätsmedizin Berlin, Germany*
[f] *Department of Mathematics, University of British Columbia, Vancouver, British Columbia, Canada*

† Electronic supplementary information (ESI) available. See DOI: **https://doi.org/10.1039/d5sm00195a**

Open Access Article. Published on 09 June 2025. Downloaded on 5/9/2026 5:04:01 AM.
This article is licensed under a Creative Commons Attribution-NonCommercial 3.0 Unported Licence.

in solvents;[5,15] it is easily understood as the longer rods have greater volume that incurs larger drag. In the v-protocol[14] and hd-protocol,[5] however, the diffusivity increases with the aspect ratio. This increase is mainly because the longer rods have smaller cross-sections in either of these protocols, and thus encounter fewer polymer chains in the gel. Thus, the OS model suggests a mechanism for the high diffusivity of thin and long rods observed experimentally.

Adhesive gels feature non-steric interactions such as hydrophobic, van der Waals, and electrostatic forces, which are essential to the filtering capability of biopolymer gels like mucus.[18] Among these, low-affinity hydrophobic interactions are particularly significant in driving adhesive behavior.[19] Posing regularly spaced discrete adhesion sites, Wang *et al.*[5] modeled the adhesive interaction with RNPs of different lengths. They uncovered an interesting non-monotonic trend for the diffusivity as a function of the RNP length in the d-protocols. Shorter RNPs tend to be captured by a single adhesive site. With increasing length, the RNP becomes increasingly susceptible to attraction toward a nearby site, which tends to dislodge it from the first site. Then the RNP moves quickly to the second adhesive site in a well-documented hopping diffusion.[5,8] This tendency yields a local maximum in diffusivity for RNPs whose length matches the spacing between adhesive sites. Even longer rods can be trapped, simultaneously and more securely, by two adhesion sites. Thus, the diffusivity decreases with greater length. When the steric repulsion is superimposed on the adhesive interaction, the diffusivity–rod-length curve gets tilted downward for the d-protocol and upward for the hd-protocol, but the local maximum persists as a hallmark of the attraction to evenly spaced adhesive sites.[5]

Since steric repulsion is at work in both adhesive and non-adhesive gels, our understanding outlined in the above relies heavily on the obstruction-scaling representation of steric repulsion. But the OS model is a phenomenological model and is not based on first principles. Therefore, further evaluation through comparison with other methods, such as numerical simulations and experiments, is necessary. In this work, we employ the Brownian dynamics (BD) method to study the transport of RNPs in hydrogels, aiming to establish a fundamental understanding of the physics. Our results suggest that in non-adhesive gels, the OS model underestimates the diffusivity of RNPs by a large margin. In adhesive gels, steric repulsion can shield the RNP from adhesive sites, thus alleviating the effect that adhesion may have on the RNP diffusion, especially for longer rods. Thus, in either type of gel, rod-like nanoparticles may enjoy an even greater advantage in rapid diffusion than previously thought.

2. Methodology

2.1. Geometric setup

To simulate the diffusion of RNPs in the gel, we construct a system composed of straight rigid polymer fibers of negligible width and rigid NPs, with the water molecules implicitly reflected by the solvent viscosity. A random network of the fibers is generated in a periodic box with side length b, containing immobile fibers of length $2L_f$. The fibers are randomly placed and oriented, creating a fibrous structure. The total number of fibers in the box is N_f, and the fiber density is $\upsilon = N_f/b^3$. Fig. 1(a) shows a schematic diagram of our simulation system. The box repeats periodically in all three dimensions such that the portion of the fibers sticking outside the box appear in it from the opposite side. Thus, the overall fiber density is maintained at the desired level. Note a simplification in our polymer network relative to a real polymer gel. Since the fibers have no thickness, they do not intersect, nor do they form physical crosslinks. Instead, the pore size is defined by the largest sphere that fits in a pore without contacting the fibers. More details will be given in Section 3.2.1.

The RNP is a spherocylinder with caps on its two ends and an aspect ratio of $\lambda = L/d$. At the start of the simulation, the RNP is randomly placed in the fiber network without intersecting any fibers. As the volume fractions in typical applications of nanoparticles are below 2%,[20] the RNPs remain in the dilute regime and do not interact with one another. Thus, we can deploy a single RNP in the periodic box and track its diffusion over a long period of time. We also include hundreds of different random realizations of the fiber network, and in each network configuration start from different initial positions and orientations of the RNP so as to construct a large ensemble of

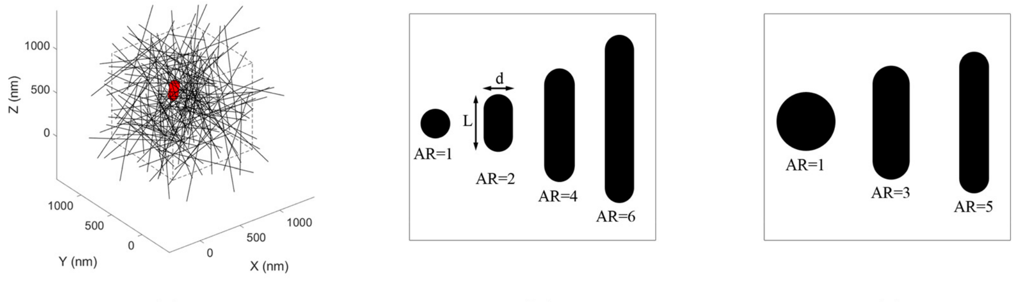

(a) (b) (c)

Fig. 1 (a) A snapshot showing a RNP (red) in a random network with $\nu = 1.6 \times 10^{20}$ m^{-3}. The dashed box shows the periodic box. RNPs with different aspect ratio values under the (b) d-protocol and (c) hd-protocol.

This journal is © The Royal Society of Chemistry 2025

Open Access Article. Published on 09 June 2025. Downloaded on 5/9/2026 5:04:01 AM.
This article is licensed under a Creative Commons Attribution-NonCommercial 3.0 Unported Licence.

thousands of diffusive trajectories. The diffusivity to be presented will come from averages over long times and large ensembles. Fig. 1(b) and (c) illustrate the d- and hd-protocols for handling the aspect ratio, respectively. Since the hd- and v-protocols yield similar nanorods, we will no longer consider the v-protocol hereafter. The hydrodynamic diameter of the RNPs, d_{H}, is calculated using the formula from Ortega and de la Torre.[21] It represents the diameter of a sphere with the same solvent diffusivity as the nanorod, allowing us to obtain d_{H} from the actual diameter (d) of the RNP:

$$\begin{aligned} d_{\mathrm{H}} &= \left(\frac{3}{2}\lambda\right)^{1/3} d\big[1.009 + 1.395\times10^{-2}\ln(\lambda) \\ &\quad + 7.88\times10^{-2}(\ln(\lambda))^2 + 6.04\times10^{-3}(\ln(\lambda))^3\big] \end{aligned} \tag{1}$$

Unless otherwise noted, the parameters used in our simulations are based on those in Wang *et al.*[5] and tabulated in Table 1. This allows for a direct comparison of our results with theirs. For the hydrodynamic diameter d_{H} = 160 nm, eqn (1) gives us the length and diameter of the RNP as the aspect ratio λ changes, and such dimensions are given in Table S1 of the ESI.† The pore size distribution of the gel is given in Fig. S1 in the ESI.† According to Ogston,[17] the average pore diameter of this network is $\bar{D} = \left(\sqrt{2\nu L_{\mathrm{f}}}\right)^{-1} = 79$ nm.

2.2. Governing equations

The translational and rotational motions of the RNPs are governed by force and torque balances. Given the scale of the problem, inertia is neglected in our simulation. The influence of the solvent is implicitly considered *via* random Brownian and drag forces and torques.[22] In our treatment of the Stokes drag force, we have neglected the hydrodynamic interaction between the RNP and the nearby polymer chains. Such interaction can potentially increase the drag on the RNP and reduce its diffusivity. But accounting for this effect would require a much more complex theoretical model.[23,24] For an axisymmetric particle, the translational motion can be decomposed into the motion in the long axis direction and the motion in a direction normal to the long axis.[25] According to Langevin's equation, the force and torque balances on a moving particle are

$$m\frac{\mathrm{d}^2\mathbf{R}^{\parallel}}{\mathrm{d}t^2} = \mathbf{F}_{\mathrm{B}}^{\parallel} - \zeta^{\parallel}\mathbf{v}^{\parallel} + \mathbf{F}_{\mathrm{ext}}^{\parallel} \approx 0, \tag{2}$$

$$m\frac{\mathrm{d}^2\mathbf{R}^{\perp}}{\mathrm{d}t^2} = \mathbf{F}_{\mathrm{B}}^{\perp} - \zeta^{\perp}\mathbf{v}^{\perp} + \mathbf{F}_{\mathrm{ext}}^{\perp} \approx 0, \tag{3}$$

$$I\frac{\mathrm{d}\boldsymbol{\omega}^{\perp}}{\mathrm{d}t} = \mathbf{T}_{\mathrm{B}}^{\perp} - \zeta^{\mathrm{r}}\boldsymbol{\omega}^{\perp} + \mathbf{T}_{\mathrm{ext}}^{\perp} \approx 0, \tag{4}$$

where m is the mass of particle, and I its moment of inertia. $\mathbf{R}$ is the center of mass of the particle, $\mathbf{v}$ is its velocity and $\boldsymbol{\omega}$ is its angular velocity. The Brownian force and torque are respectively $\mathbf{F}_{\mathrm{B}}$ and $\mathbf{T}_{\mathrm{B}}$, and $\mathbf{F}_{\mathrm{ext}}$ and $\mathbf{T}_{\mathrm{ext}}$ are external force (*e.g.*, steric repulsion) and torque on the particle. For all the vectors, the superscripts $\parallel$ and $\perp$ mark their components parallel and normal to the particle axis direction, respectively. For example, $\mathbf{F}_{\mathrm{ext}}^{\parallel}(t) \equiv [\mathbf{F}_{\mathrm{ext}}(t)\cdot\mathbf{\Omega}(t)]\mathbf{\Omega}(t)$, $\mathbf{\Omega}(t)$ being the unit vector along the axis of the RNP, and $\mathbf{F}_{\mathrm{ext}}^{\perp}(t) = \mathbf{F}_{\mathrm{ext}}(t) - \mathbf{F}_{\mathrm{ext}}^{\parallel}(t)$. The translational and rotational drag coefficients are related to the respective diffusivities *via* the Stokes–Einstein relation: $\zeta^{\parallel} = k_{\mathrm{B}}T/D_0^{\parallel}$, $\zeta^{\perp} = k_{\mathrm{B}}T/D_0^{\perp}$, $\zeta^{\mathrm{r}} = k_{\mathrm{B}}T/D_0^{\mathrm{r}}$, with $k_{\mathrm{B}}T$ being the thermal energy and $D_0^{\perp}$, $D_0^{\parallel}$ and D_0^{r} being the parallel translational, normal translational and rotational diffusivity in the solvent, given by the following formulae:[26–28]

$$D_0^{\perp} = \frac{\psi}{4\pi}\left(\ln\lambda + 0.839 + 0.185/\lambda + 0.233/\lambda^2\right) \tag{5}$$

$$D_0^{\parallel} = \frac{\psi}{2\pi}\left(\ln\lambda - 0.207 + 0.980/\lambda - 0.133/\lambda^2\right) \tag{6}$$

$$D_0^{\mathrm{r}} = \frac{3\psi}{\pi L^2}\left(\ln\lambda - 0.662 + 0.917/\lambda - 0.050/\lambda^2\right) \tag{7}$$

with

$$\psi = k_{\mathrm{B}}T/\mu L \tag{8}$$

where μ the viscosity of the solvent. The overall solvent diffusivity can be defined as $D_0 = (1/3)(2D_0^{\perp} + D_0^{\parallel})$. In all simulations, we set T = 300 K and μ = 1 cP.

The Brownian force components $\mathbf{F}_{\mathrm{B}}^{\parallel} = F_{\mathrm{B}}^{\parallel}\mathbf{\Omega}$ and $\mathbf{F}_{\mathrm{B}}^{\perp} = F_{\mathrm{B}}^{\perp 1}\mathbf{e}_1 + F_{\mathrm{B}}^{\perp 2}\mathbf{e}_2$, where $\mathbf{e}_1$ and $\mathbf{e}_2$ are two orthogonal unit vectors perpendicular to $\mathbf{\Omega}$, have the following stochastic characteristics:

$$\langle F_{\mathrm{B}}^{\parallel}(t)\rangle = 0, \quad \langle F_{\mathrm{B}}^{\parallel}(t)F_{\mathrm{B}}^{\parallel}(t')\rangle = 2\zeta^{\parallel}k_{\mathrm{B}}T\delta(t-t') \tag{9}$$

$$\begin{aligned} \langle F_{\mathrm{B}}^{\perp 1}(t)\rangle = \langle F_{\mathrm{B}}^{\perp 2}(t)\rangle = 0, \quad \langle F_{\mathrm{B}}^{\perp 1}(t)F_{\mathrm{B}}^{\perp 1}(t')\rangle &= \langle F_{\mathrm{B}}^{\perp 2}(t)F_{\mathrm{B}}^{\perp 2}(t')\rangle \\ &= 2\zeta^{\perp}k_{\mathrm{B}}T\delta(t-t') \end{aligned} \tag{10}$$

in which $\delta(t-t')$ is the Dirac delta function. Similarly, the Brownian torque has the following stochastic characteristics:

$$\begin{aligned} \langle T_{\mathrm{B}}^{\perp 1}(t)\rangle = \langle T_{\mathrm{B}}^{\perp 2}(t)\rangle = 0, \quad \langle T_{\mathrm{B}}^{\perp 1}(t)T_{\mathrm{B}}^{\perp 1}(t')\rangle &= \langle T_{\mathrm{B}}^{\perp 2}(t)T_{\mathrm{B}}^{\perp 2}(t')\rangle \\ &= 2\zeta^{\mathrm{r}}k_{\mathrm{B}}T\delta(t-t') \end{aligned} \tag{11}$$

The discretization scheme of the governing equations is detailed in Section S2 of the ESI.†

Table 1 Typical parameters for the RNPs and the hydrogel

Parameters	Value	Explanation
$2\nu L_{\mathrm{f}}$	16×10^{13} m^{-2}	Total fiber length per unit volume
$2L_{\mathrm{f}}$	1 μm	Length of the fibers
d_{H}	160 nm	Hydrodynamic diameter of NPs

2.3. Steric interaction

The steric effect is implemented using the Lennard-Jones (LJ) potential. We have also tested two others models to confirm that the specific details of the interaction potential or force do

Open Access Article. Published on 09 June 2025. Downloaded on 5/9/2026 5:04:01 AM.
This article is licensed under a Creative Commons Attribution-NonCommercial 3.0 Unported Licence.

not significantly affect our results. The details of these models are given below.

2.3.1. Lennard-Jones potential. The steric repulsion is modeled by a truncated and shifted LJ potential U_s, such that the steric repulsion force is given by $\mathbf{F}_s = -\nabla U_s$:[18]

$$U_s(\delta) = \sum_{n=1}^{N_f} \begin{cases} 4\varepsilon\left[\left(\frac{s}{2\delta}\right)^{12} - \left(\frac{s}{2\delta}\right)^{6} + \frac{1}{4}\right], & \delta \le 2^{-\frac{5}{6}}s \\ 0, & \delta > 2^{-\frac{5}{6}}s \end{cases} \tag{12}$$

where $\varepsilon = 1k_BT$ is the energy depth, δ the center-to-center distance between the RNP and the fiber, and $s = d + d_f = d$ is the steric diameter, as the fibers have zero thickness: $d_f = 0$.

2.3.2. Chen's model. To represent steric repulsion, Chen *et al.*[29] proposed an alternative formulation. The repulsive force acting on the RNP is given as follows:

$$\mathbf{F}^{\text{rep}} = F^{\text{rep}} e^{\frac{-h}{k_{\text{steric}}}} \mathbf{n},\, h < h^{\text{cutoff}} \tag{13}$$

and the associated torque on the RNP is

$$\mathbf{T}^{\text{rep}} = \mathbf{G} \times \mathbf{F}^{\text{rep}} \tag{14}$$

where $\mathbf{n}$ is the direction normal to both surfaces, $k_{\text{steric}} = d/40$ is the interaction range, h is the shortest separation between object surfaces, $h^{\text{cutoff}} = 0.66 \times d$ is the cutoff distance, $\mathbf{G}$ is the moment arm, and $F^{\text{rep}} = 900\pi\mu r_p{}^2(\lambda - 1)D_0^r$ is the repulsive force scale. It should be noted that unlike the LJ potential that is based on the center-to-center distance, Chen's model is based on the surface-to-surface distance.

2.3.3. Monte Carlo scheme. Finally, we have also tested a Monte Carlo acceptance/rejection procedure. At each Monte Carlo step, we generate a random Brownian force and torque from eqn (9)–(11), and move the RNP to a new position and orientation according to eqn (2)–(4), but with the external force $\mathbf{F}_{\text{ext}}$ and $\mathbf{T}_{\text{ext}}$ set to zero. Then we check if the new position and orientation would result in the RNP overlapping any fiber. In the event of an overlap, the step is rejected, and the RNP stays at the current position to wait for the next time step.[30] If no overlap, the new RNP position and orientation is accepted.

2.4. Adhesive interactions

To capture the adhesive interaction between the RNP and the fiber network, we adapt the treatment of Wang *et al.*[5] in one and three dimensions to the three-dimensional geometry of our Brownian dynamics simulation. Although multiple physical mechanisms can induce NP–gel adhesion, the modeling here is based on the physical picture of hydrophobic interactions with discrete sites on the polymer backbones. Other types of adhesive forces, *e.g.*, electrostatic or van der Waals forces, can be easily incorporated through appropriate forms of the interaction potential below.[31]

Following Wang *et al.*,[5] we assume discrete adhesion sites on the fiber network. To describe the adhesion between one such site and a unit length of a nearby RNP, we adopt a Morse potential:

$$U(x) = U_0(e^{-2x/\rho} - 2e^{-x/\rho}) \tag{15}$$

where U_0 is the adhesion strength, x is the distance between the fibers' adhesion sites and the unit length of the RNP, and ρ the potential range, to which we assign the value of 20 nm following Wang *et al.*[5] The total adhesion energy is the integral of $U(x)$ over the axial length of the RNP. For such an integration, we discretize the RNP length into segments 10 nm in length. Thus, there are from 14 to 33 such axial segments along the RNP depending on the aspect ratio λ (Table S1, ESI†). We have run numerical experiments to verify that this RNP discretization is fine enough so as to not to affect the results in any significant way. Details of this verification can be found in Section S3 of the ESI.†

The main difference from Wang *et al.* adhesion model lies in the positioning of the adhesion sites on the 3D random fiber network. This is accomplished in two steps. First, we uniformly place the adhesion sites onto a regular cubic lattice inside the simulation box, with equal separation of r_0 = 200 nm (Fig. 2(a)). This layout is identical to the 3D lattice employed by Wang *et al.*[5] Second, we reposition the adhesion sites onto the random fiber network by shifting each site to the nearest point on the closest fiber (Fig. 2(b)). Thus, the adhesion sites all fall on the fibers but exhibit a roughly uniform spatial distribution. In a real gel, of course, the adhesion sites may not be uniform.

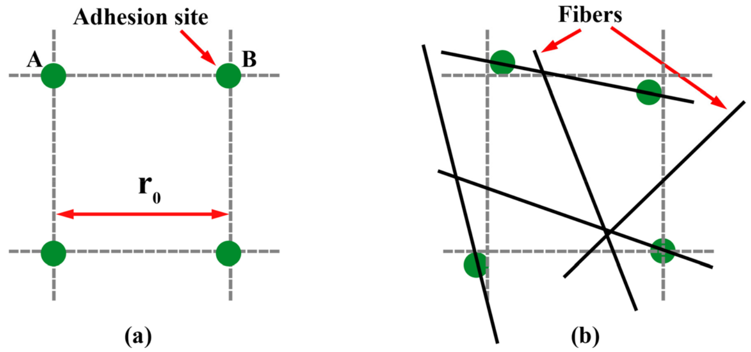

Fig. 2 (a) Schematic illustrating adhesion sites positioned at the vertices of a 3D regular network. (b) The adhesion sites are repositioned to the nearest points on the closest fibers, ensuring they are located on the fiber. The dashed lines are included as a guide to the eye.

This journal is © The Royal Society of Chemistry 2025

Open Access Article. Published on 09 June 2025. Downloaded on 5/9/2026 5:04:01 AM.
This article is licensed under a Creative Commons Attribution-NonCommercial 3.0 Unported Licence.

Given our focus on the RNP shape, however, we will not probe the effects of the density and spatial heterogeneity of the adhesion sites.

Our numerical algorithm follows standard Brownian dynamics procedures. The temporal discretization scheme for integrating the Langevin equation is detailed in the ESI† (Section S2), as are the procedures for evaluating statistical quantities of interest, such as the mean square displacement (MSD) and the diffusivities, from the RNP trajectories (Section S4, ESI†).

3. Results & discussion

3.1. Validation of the model

To test the validity of our physical model and the accuracy of our numerical algorithm, we have simulated three simpler situations where a benchmark is available for comparison. First, we compute the translational and rotational diffusivities of nanorods of cross-sectional diameter d = 80 nm and various lengths in a pure solvent with μ = 1 cP, T = 300 K. Compared with the analytical relations of Tirado *et al.*[27] (see eqn (5)–(8)), both show close agreement (Fig. 3(a) and (b)). This confirms that we have correctly implemented the discrete Brownian force in our model, and the numerical parameters used, including the time step Δt, number of particles P, total time of simulation, sampling protocols, ensure adequate resolution and accuracy in our code. We have previously tested these numerical parameters for SNPs in our previous work,[2] and similar tests have been done for RNPs here. Details are not given for brevity.

We further validate our model *via* Brownian dynamics simulation of Chen *et al.*[29] of the interactions between RNPs with d = 5.6 nm and λ = 5. They are suspended in a quiescent liquid medium of viscosity μ = 1 cP, and their diffusion under a Brownian force is tracked in time for evaluating the translational and rotational diffusivities. To replicate their results, we employed Chen's model for the steric repulsion (eqn (13) and (14)). For volume concentration of up to 38%, our model accurately reproduces the literature data (Fig. 3(c) and (d)).

Finally, we reduce our model to account for the diffusion of SNPs, as Ogston[17] has developed an OS model for such SNPs diffusing in a non-adhesive random polymer network. This model yields the following formula for the diffusivity of

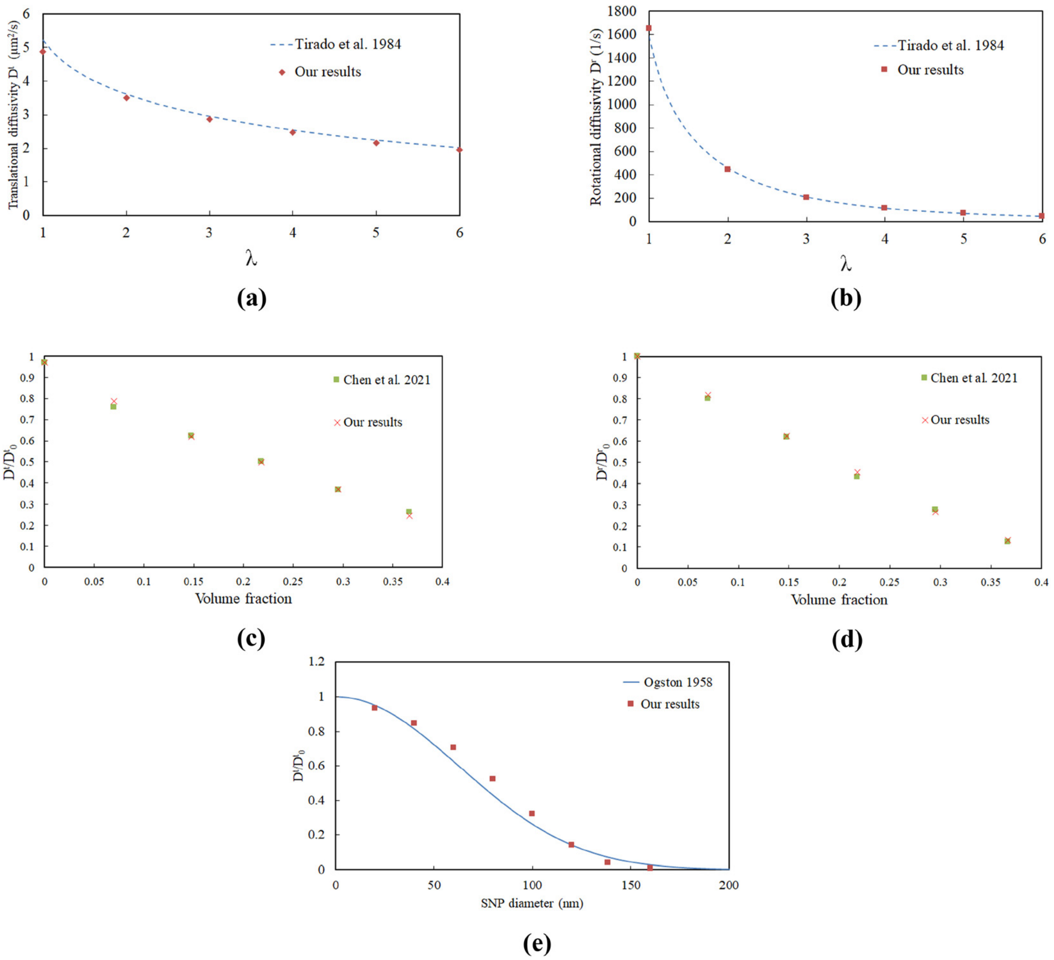

(a) (b) (c) (d) (e)

Fig. 3 Comparison between our simulations and (a) and (b) analytical relations proposed by Tirado *et al.*[27] in a pure solvent with μ = 1 cP, T = 300 K as a function of RNP aspect ratio (c) and (d) an existing BD study by Chen *et al.*[29] under rod–rod interaction as a function of volume fraction where d = 5.6 nm and λ = 5, (e) Ogston's OS model[17] in a non-adhesive random gel as a function of SNP size. In this model, $2L_f$ = 1 μm and $\nu = 1.6 \times 10^{20}$ m^{-3}.

Open Access Article. Published on 09 June 2025. Downloaded on 5/9/2026 5:04:01 AM.
This article is licensed under a Creative Commons Attribution-NonCommercial 3.0 Unported Licence.

the SNP as a function of its diameter:

$$D/D_0 = \exp\left(-\frac{\pi\nu L_\mathrm{f} d^2}{2} - \frac{\pi}{6}\nu d^3\right) \tag{16}$$

As shown in Fig. 3(e), our results align well with Ogston's equation. Together, these three validations demonstrate that our model can accurately predict the diffusion of both RNPs and SNPs in non-adhesive gels.

3.2. Diffusion in non-adhesive gels: effect of aspect ratio

We study the diffusion of RNPs in random and non-adhesive gels by varying their aspect ratio in the hd-protocol. The main finding of this work is shown in Fig. 4 with the translational diffusivity as a function of the aspect ratio. Both our model, incorporating different repulsive potentials for steric interaction, and Wang's extended OS model[5] show that the diffusivity of RNPs increases monotonically with the aspect ratio. This increase has been attributed to the cross-sectional area of the RNP:[5] rods with a smaller λ have larger cross-sections which may impede their passage through the pores. Surprisingly, our BD model predicts much higher diffusivities compared to Wang's model, with the discrepancy becoming more pronounced as the RNPs become longer and thinner. As a check on our BD results using the LJ potential (eqn (12)), we have repeated the simulations using two alternative representations of the steric repulsion: the repulsive force of Chen *et al.*[29] (eqn (13)) and the Monte Carlo scheme described in Section 2.3.3. All three results agree closely, with a much higher D^t than predicted by the OS model. We also numerically integrated Wang's model (eqn (6) and (7) in their paper) and successfully reproduced their reported results. Therefore, we conclude that the discrepancy is not due to errors. Rather it reflects substantive differences between the two models.

The OS model centers on the probability of the RNP overlapping a polymer chain if it were inserted into the gel at a randomly chosen centroid position and a random orientation. This probability is a purely geometric property, and can be calculated from the known location and orientation of all the polymer chains.[5] More specifically, in a large ensemble of repeated random insertion of the RNP into the gel, one counts the percentage of the insertions with the RNP encountering no fiber. This probability p is then equated to the relative diffusivity $D_\mathrm{g}/D_0 = p$.

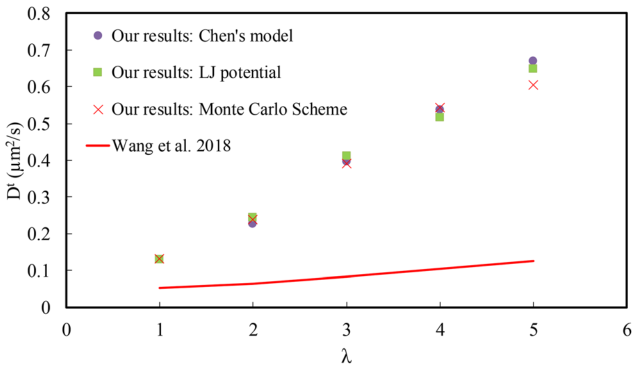

Fig. 4 Comparison between our simulations, employing different steric models, and Wang's OS model as a function of aspect ratio. The parameters used here are listed in Table 1.

Our Brownian dynamics simulation tracks the continuous movement of the RNP through the pores of the network. Thus, the obstruction that it experiences from the polymer chains depends on its continuous trajectory and may well differ from that of an RNP repeatedly inserted into the gel, with no correlation of the RNP position and orientation from one trial to the next. More specifically, the diffusing RNP may linger in certain regions while speeding through other regions. It may even be excluded from certain pores. Fig. 5(a) and (b) compare the distribution of the RNP centroid for the successful insertions in the protocol of the OS model with that from diffusing RNPs in our Brownian dynamics simulation. In recording the location of successful RNP insertions without intersecting any fiber, panel (a) essentially presents a "negative" of the fiber density distribution or pore size distribution. Comparing the two plots, we notice similarities; in both cases, the RNP ends up more often in coarse regions with larger pores. But panel (b) is more spatially heterogeneous than (a), with the dark and blank areas more sharply delineated and separated from each other. Some regions with smaller pores, sparsely populated in (a), are not visited at all by the diffusing RNP in (b). The existence of such small "dead pores" implies that the RNP experiences a lower effective crowdedness than given by the overall fiber density. Equivalently, the difference between (a) and (b) suggests that the diffusing RNP lingers more in the coarser regions of the gel than the denser regions, thus amplifying the contrast between regions of low and high fiber density. Evidently, the diffusion trajectory samples a fiber distribution that is skewed from that experienced by a randomly inserted RNP. This qualitative observation is quantified in Fig. 5(c), which compares the distribution of nearest neighbor distances for the two models. In the BD simulation, the peak of the nearest-neighbor distance distribution occurs at a smaller value compared to the OS model, indicating a more compact particle distribution. In contrast, the OS model exhibits a longer tail towards larger distances, reflecting a sparser distribution of nanoparticles across the gel. Thus, the histogram provides numerical evidence for the amplified spatial heterogeneity seen in the BD simulation.

3.2.1. Two modes of diffusion.

We have analyzed typical BD trajectories to gain insights into the behavior of the RNP within the system. Of the large number of simulations that we have done, all exhibit the common feature that the trajectory consists of episodes in two distinct modes of motion, which we call the "meandering diffusion" and "directional diffusion", respectively. Representative episodes in these two modes are shown in Fig. 6(a) and (b). Note that all episodes are chosen to be of equal duration. In the meandering phase, the trajectory appears as a dense cloud, with frequent changes in direction and short displacements in between. In contrast, the directional diffusion is marked by a rapid traversal of space within a relatively short time. The trajectory thus appears to be sparse

Open Access Article. Published on 09 June 2025. Downloaded on 5/9/2026 5:04:01 AM.
This article is licensed under a Creative Commons Attribution-NonCommercial 3.0 Unported Licence.

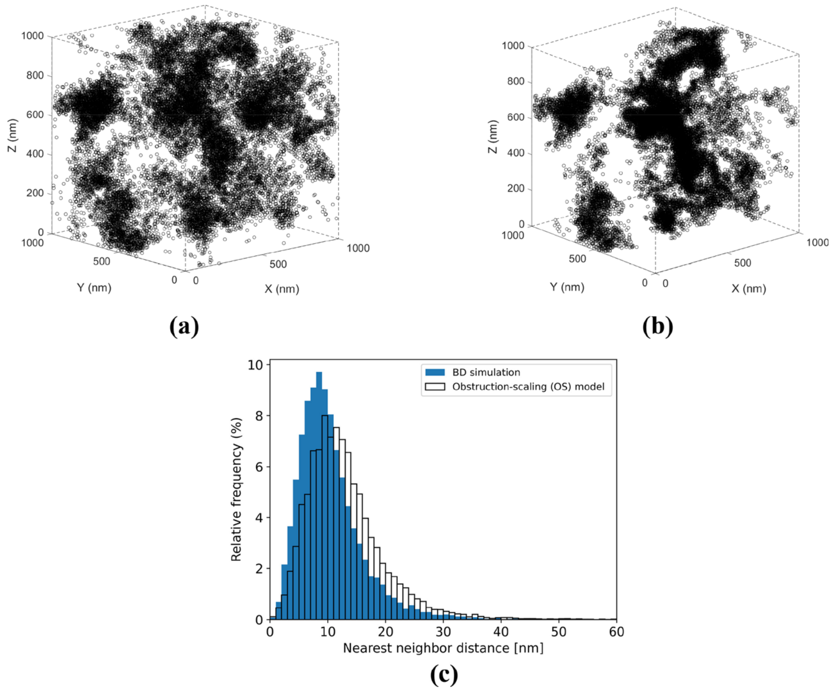

Fig. 5 Distribution of center of mass of nanorods in (a) random toss in the free space of the gel and (b) our BD simulations. Each graph has 20 000 data points and these distributions are obtained in the same gel. Fibers are not shown for the sake of clarity. (c) Histogram showing the distribution of nearest neighbor distances for our BD simulation and the OS model. The relative frequency is the percentage of nearest neighbor pairs with distance in each of 60 brackets relative to the total number of pairs.

and elongated, with relatively long stretches between changes of direction. This suggests a higher translational diffusivity for the directional mode, a feature to be demonstrated below. The distinction between the two modes of diffusion can be made more quantitative by evaluating the density of neighboring points on the RNP trajectory. This has been done using two different metrics, and the details can be found in the ESI,† Section S5. Incidentally, the directional diffusion is reminiscent of the "rapid sliding mode of diffusion" identified by Zhang *et al.*[12] for short rods, due to the entropic penalty against the rods perturbing the conformation of the flexible polymer chains. Our directional diffusion, as will be demonstrated below, arises from an entirely different mechanism.

It turns out that the meandering mode occurs in coarser regions of the gel with larger pore sizes, and the directional mode in denser regions with smaller pore sizes. To demonstrate this, we enclosed the above trajectories in cuboids, in which the pore size and fiber crowdedness can be evaluated. To calculate the pore size, we follow a procedure adapted from Stylianopoulos *et al.*[32] First, we randomly select a point inside the box that is not occupied by fibers. Then, we calculate the maximum diameter of a sphere centered at the selected point that does not touch any fiber. This is repeated over 50 000 points and the average is taken. The results reveal that the ensemble-averaged pore diameter is about 125 nm in the meandering mode and 100 nm in the longitudinal mode. These findings support the notion that the meandering and directional modes occurred in coarser and denser regions, respectively.

Following Zhao *et al.*,[14] we define a crowdedness number N to characterize the proximity of the fibers around the RNP. For this purpose, we discretize each fiber into n_f equally spaced "beads", and similarly the RNP into n_r beads. This *ad hoc* segmentation is specific to this calculation and does not affect the BD model. We calculate a crowdedness number $N(t)$ as follows:

$$N(t) = \sum_{i}^{n_\mathrm{r}} n_i \tag{17}$$

where n_i denotes the number of fiber beads within the cutoff distance l_e = 200 nm from the RNP bead i, and each bead on the fibers is only counted once. Fig. 6(c) shows the variation of $N(t)$ as a function of time for the ten trajectories shown in Fig. 6(a) and (b) for each mode of motion. As it can be seen, $N(t)$ is generally higher during the longitudinal mode of diffusion, thus confirming the pore-size comparison above that the RNP executes longitudinal diffusion in more crowded regions and meanders in less crowded regions. We have done numerical experiments by varying n_f, n_r and l_e to ensure that this trend does not depend on these parameters; see Section S6 of the ESI† for details.

3.2.2. **Residence time.** The diffusing RNP, as it turns out, spends about 75% of its time in the meandering mode. The identification of meandering and directional episodes and the estimation of their durations are carried out using the density-based spatial clustering of applications with noise (DBSCAN) algorithm and Voronoi tessellation. Both methods give highly consistent conclusions over multiple trajectories, some of

Open Access Article. Published on 09 June 2025. Downloaded on 5/9/2026 5:04:01 AM.
This article is licensed under a Creative Commons Attribution-NonCommercial 3.0 Unported Licence.

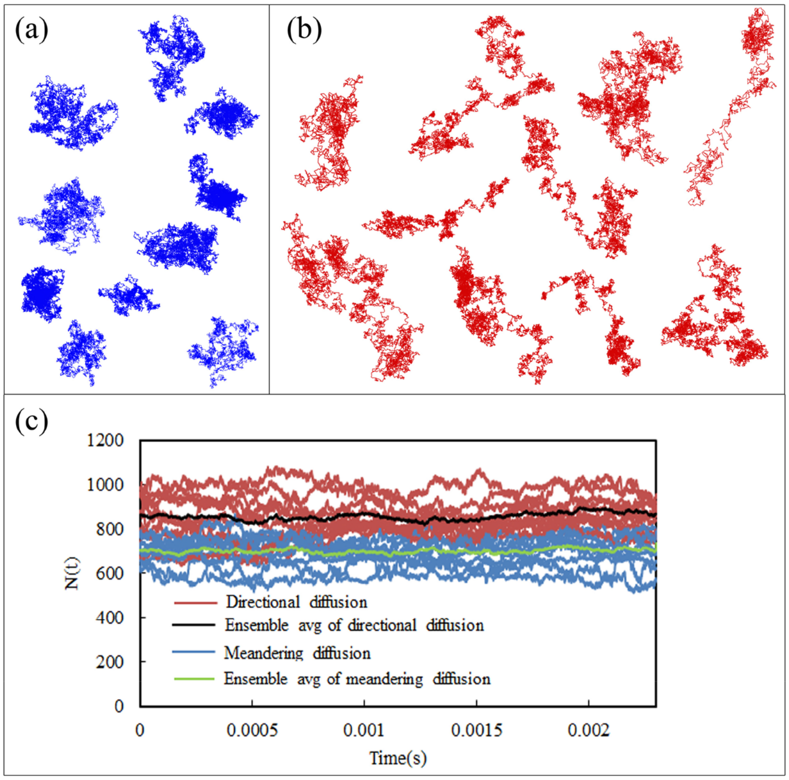

Fig. 6 Typical trajectories of rods exhibiting (a) meandering and (b) directional diffusion. (c) The evolution of $N(t)$ as a function of time for the trajectories shown in (a) and (b). The start of each trajectory is shifted to $t = 0$ to facilitate comparison. The ensemble-averaged $N(t)$ for the ten trajectories in each mode is also shown.

which are shown in Fig. S3 (ESI†). More details are given in Section S5 of the ESI.†

The implication is clear: the RNP spends more time in the coarser region of the gel while undergoing meandering diffusion and traverses the denser regions briefly in directional diffusion. Judging from the residence time, we clearly see a bias in how the RNP experiences the fiber network; it prefers to linger in the coarser regions with larger pores, and thus samples a pore-size distribution along its diffusive trajectory that is skewed in favor of larger pores. This provides quantitative support to the visual observations in Fig. 5. An immediate consequence of this observation is that the RNP will exhibit an overall translational diffusivity that corresponds to an effectively coarser gel with larger pores. This provides a plausible explanation for the discrepancy in Fig. 4; our BD simulation should indeed produce a higher D^t than that predicted by the OS model using the static pore size distribution.

3.2.3. Anisotropic diffusion. In addition to the skewed pore-size distribution, another factor further elevates the translational diffusivity of the RNP: the anisotropy of its shape leads to anisotropy in its diffusion. This can be appreciated first from the negative correlation between the rotational and translational diffusivities, and second from an anisotropic factor on the RNP displacement.

In the coarser regions of the gel, the RNP can rotate more freely and have access to a wider range of directions for its diffusion. In contrast, in denser regions, their rotation and transverse diffusion are severely curtailed. As a consequence, the RNP is more liable to diffuse longitudinally, with little rotation or lateral translation. This distinction is illustrated by the cartoons of Fig. 7. As is well known, the longitudinal motion enjoys smaller viscous drag and faster diffusion. This is consistent with the previous observation that the RNP lingers in the coarser regions undergoing meandering diffusion, and rapidly traverses the denser regions in directional diffusion.

To quantify the idea above, we compute a "local" translational and rotational diffusivity. At time t, we define the local mean squared displacement (LMSD) and the local translational diffusivity D_l^t by tracing back M time steps:[33]

$$\text{LMSD}(t) = \langle[(r(t) - r(t - M\Delta t))^2]\rangle \tag{18}$$

$$D_\text{l}^\text{t} = \frac{\langle\text{LMSD}\rangle}{6M\Delta t} \tag{19}$$

Similarly, the local rotational diffusivity D_l^r is defined as

$$D_\text{l}^\text{r} = \left(\frac{-1}{2M\Delta t}\right)\ln[\langle\Omega(t)\cdot\Omega(t - M\Delta t)\rangle] \tag{20}$$

The local translational and rotational diffusivities, along with their corresponding distributions, are plotted in Fig. 8 for the trajectory shown in Fig. 6. The longitudinal motion features a higher translational diffusivity but a lower rotational diffusivity, while the opposite is true for the meandering motion. For example, the time- and ensemble-averaged

Open Access Article. Published on 09 June 2025. Downloaded on 5/9/2026 5:04:01 AM.
This article is licensed under a Creative Commons Attribution-NonCommercial 3.0 Unported Licence.

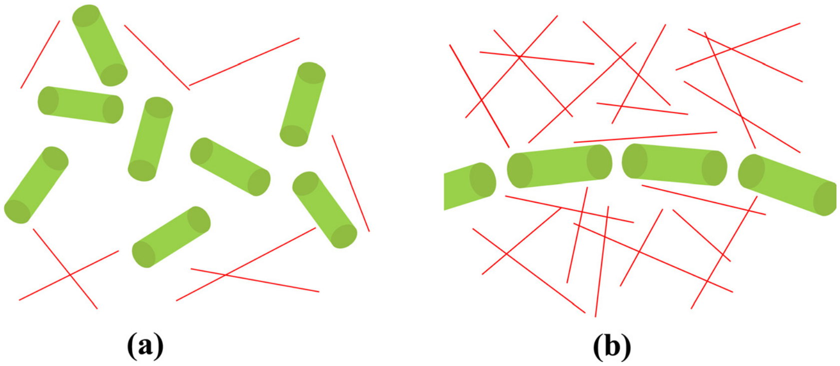

Fig. 7 Schematic illustration of (a) the meandering diffusion of nanorods in a coarser region of the gel, and (b) the directional diffusion in a denser region.

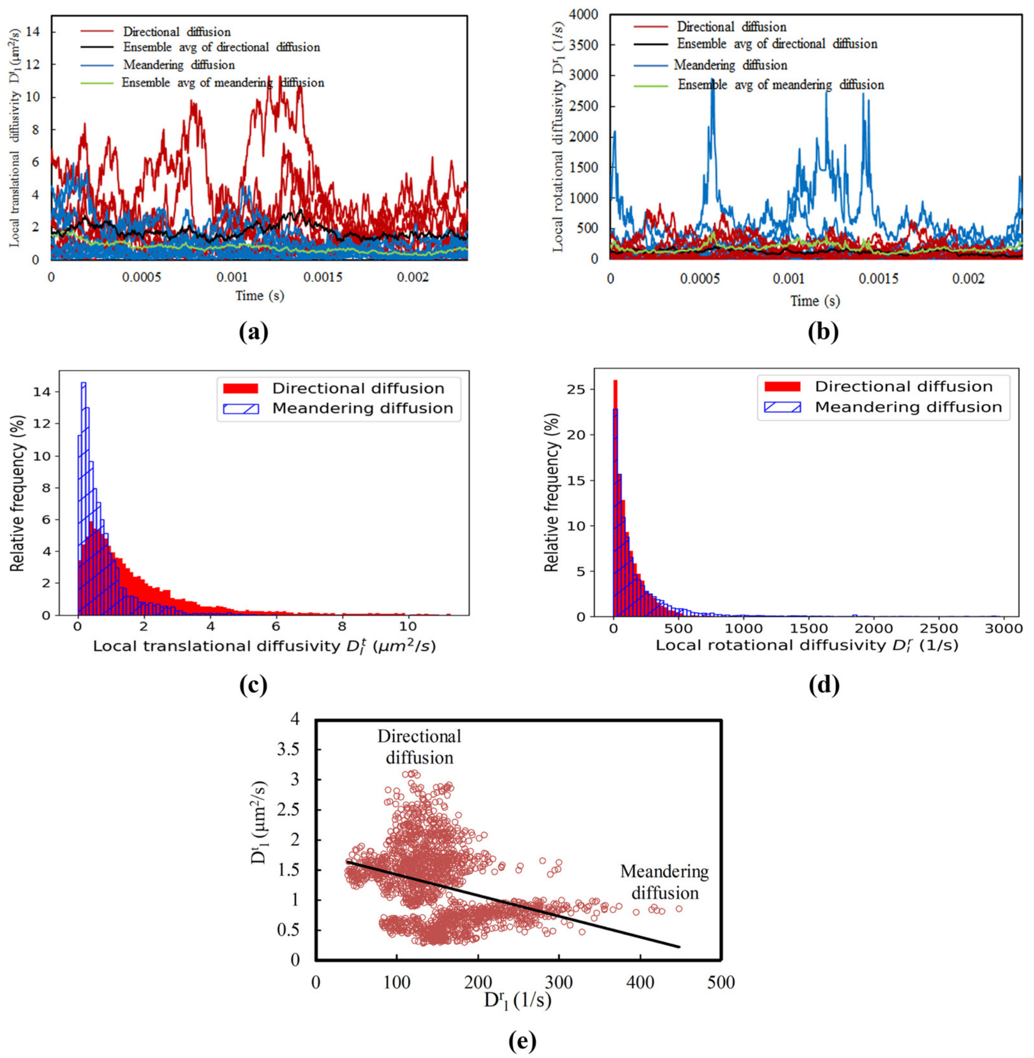

Fig. 8 The evolution of (a) the local translational diffusivity D_l^t and (b) the local rotational diffusivity D_l^r as a function of time for the trajectories shown in Fig. 6. (c) and (d) Histograms showing the corresponding distributions of the local translational and rotational diffusivities. (e) Scatter plot of D_l^t *versus* D_l^r for the ensembled averaged data, with a linear regression showing the negative correlation: $D_l^t = -0.0034D_l^r + 1.7726$.

translational diffusivity for the directional diffusion is 1.75 $\mu m^2\ s^{-1}$, 2.3 times higher than that of the meandering diffusion (0.75 $\mu m^2\ s^{-1}$). The trend is reversed for the rotational diffusivity: the meandering mode exhibits a higher average value of 181 s^{-1} compared to 123 s^{-1} for the directional mode. The same trend is demonstrated by the distributions of D_l^t and D_l^r in Fig. 8(c) and (d).

Open Access Article. Published on 09 June 2025. Downloaded on 5/9/2026 5:04:01 AM.
This article is licensed under a Creative Commons Attribution-NonCommercial 3.0 Unported Licence.

These histograms are obtained by sampling the diffusivity values from the 10 individual trajectories of Fig. 8(a) and (b), dividing the range of the diffusivity into 100 bins, and counting the occurrence in each bin as a percentage of the total counts over all the bins. Clearly, the meandering mode tends to have a lower D_l^t and a higher D_l^r than the directional mode. The negative correlation between the rotational and translational diffusion (Fig. 8(e)) has a correlation coefficient

$$\mathrm{corr} = \frac{\Sigma(x_i - \bar{x})(y_i - \bar{y})}{\sqrt{\Sigma(x_i - \bar{x})^2 \Sigma(y_i - \bar{y})^2}} = -0.328. \qquad (21)$$

This forms an interesting contrast with the observation of a positive correlation by Xue *et al.*[11] in a highly uniform gel. Our mechanism relies on spatial fluctuations of fiber concentration and pore size in our random gel, which are absent in their context.

In addition, we employ the local anisotropic diffusion parameter $A(t)$, introduced by Zhao *et al.*,[14] to characterize the anisotropy of diffusion:

$$A(t) = \frac{3\mathrm{LMSD}_{\parallel}(t)}{\mathrm{LMSD}(t)} - 1 \qquad (22)$$

where $\mathrm{LMSD}_{\parallel} = \langle((r(t) - r(t - M\Delta t))\cdot\Omega(t - M\Delta t))^2\rangle$ represents the component of the LMSD parallel to the major axis of the RNP. Thus, the parameter $A(t)$ quantifies the prevalence of longitudinal diffusion, with $A(t) = 0$ for isotropic diffusion, and $A(t) = 2$ for completely unidirectional longitudinal diffusion. For what we have called the "directional phase" of the trajectory, the time- and ensemble-averaged A is 0.609, which is about nine times larger than in the "meandering phase" ($A = 0.067$). Taken together, the above findings complement one another to produce an elevated translational diffusivity for RNPs than expected from OS models. One aspect of the RNP diffusion, that the directional mode enjoys greater translational diffusivity than the meandering mode, seems natural. But two other aspects may seem counterintuitive: that the meandering mode occurs in the coarser region of the gel with larger pore sizes, and that the RNP spends more time in the coarser areas than in the denser ones. Our intuition has largely come from the diffusion of SNPs, which are known to spend long periods in a dense "cage", where they execute slow and meandering diffusion, before a brief and rapid "escape" through coarse regions of the gel.[34] For RNPs, on the other hand, their anisotropy in shape engenders anisotropy in diffusion, as illustrated in the above by the anisotropy parameter A and the negative correlation between rotational and translational diffusivities. This explains the unexpected and distinct trends for the diffusion of RNPs.

The OS model has long been the primary conceptual framework for understanding NP diffusion in polymer networks. However, our BD simulations have revealed its limitations: the OS model relies solely on the static geometry of the network and fails to account for the dynamic, continuous trajectories of diffusing NPs. For spherical NPs, this connectivity factor is largely negligible, and the OS model predicts SNP diffusivity with good accuracy (Fig. 3(e)). For rod-like NPs, however, the discrepancy is amplified by the anisotropy in diffusion, and grows with the aspect ratio (Fig. 4). This finding underscores the value of our work.

3.3. Comparison with experimental data

Can the discrepancy between our BD results and the prediction of the OS model be further assessed by comparison with experimental data? We find that quantitative comparison is hampered by a dearth of pertinent data, but qualitative ones can be made. Wang *et al.*[5] conducted experiments on the diffusion of silica nanorods in 0.5 wt% hydroxyethyl cellulose (HEC) gel in water. This is a hydrophilic and non-ionic gel without hydrophobic regions, and a good model for a non-adhesive gel. We have chosen our model parameters to match the experimental system. The fiber length is set to $2L_f = 1\ \mu\mathrm{m}$, a reasonable length in view of literature data.[35] To estimate the fiber density (ν), we fitted the OS model to the experimental data at a single point: $\lambda = 1$, corresponding to an 80 nm SNP. This yields $\nu = 9.84 \times 10^{20}\ \mathrm{m}^{-3}$. In the OS model, the diffusivity depends only on the product νL_f, rather than the individual values of ν and L_f, as long as L_f is much longer than the pore sizes. We have tested different combinations of L_f and ν to ensure the robustness of our numerical parameters. The BD simulations produced essentially identical diffusivities across all combinations, confirming that the results are insensitive to the assumed fiber length L_f. Note that the ν chosen to compare with the experiments is more than six times that of Table 1 and Fig. 4.

Using the extended OS and our BD model, we have computed the translational diffusivity for a range of λ values using the d-protocol, as the experiments were for a series of RNPs with the same cross-sectional diameter and increasing length. Fig. 9 compares the experimental data with predictions of both models. Both models capture the correct trend of D^t decreasing with λ in the d-protocol, but both underpredict D^t. Our model predicts a higher D^t that is closer to the experimental data over the entire λ range, except for the starting point at $\lambda = 1$.

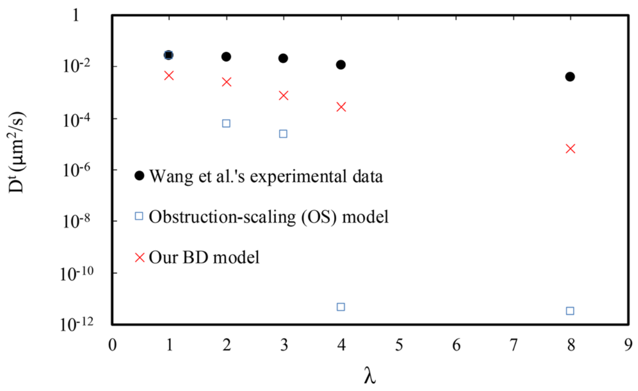

Fig. 9 Comparison between Wang *et al.* experimental data[5] and the predictions of their OS model and our BD model for different aspect ratio values. In this comparison, $2L_f = 1\ \mu\mathrm{m}$ and $\nu = 9.84 \times 10^{20}\ \mathrm{m}^{-3}$.

Open Access Article. Published on 09 June 2025. Downloaded on 5/9/2026 5:04:01 AM.
This article is licensed under a Creative Commons Attribution-NonCommercial 3.0 Unported Licence.

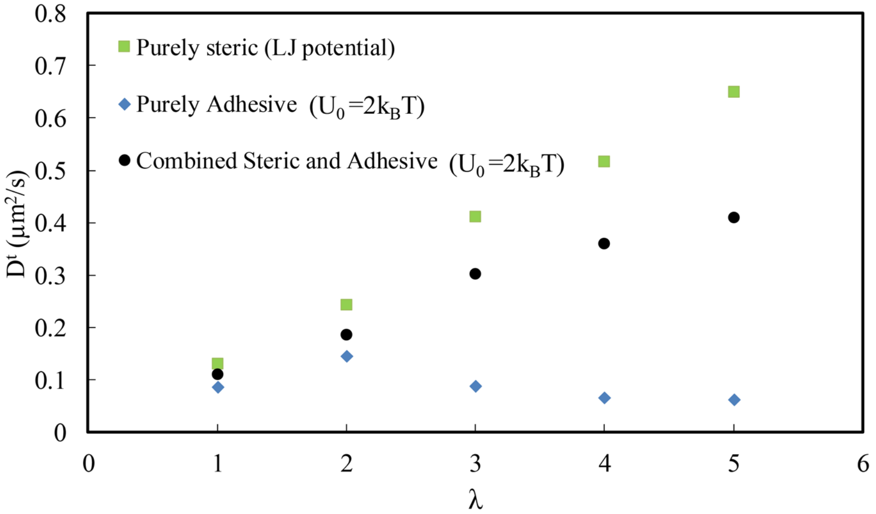

Fig. 10 Translational diffusivity as a function of aspect ratio λ under the hd-protocol (d_H = 160 nm) with purely steric interactions, purely adhesive interactions, and their combination. The nominal separation between neighboring adhesion sites is r_0 = 200 nm.

This comparison, if not quantitatively conclusive, suggests that our model outperforms the OS model for RNPs. The higher diffusivity observed in the experiments can perhaps be attributed to the flexibility of both the nanorods and fibers in the experimental setup.[36] Both models assume the rods and fibers to be rigid. Note that at λ = 1, the OS model is fitted to the experimental data to generate the model parameters. For such parameters, the BD model yields a slightly smaller D^t at λ = 1. Had we fitted that data point to our BD model, its predicted D^t would have been even closer to the experimental measurements for $\lambda > 1$.

3.4. Diffusion in adhesive gel

To understand the diffusion of RNPs under the combined effects of steric and adhesive interactions, it is convenient to first examine each interaction independently. Fig. 10 compares the RNP translational diffusivity in three scenarios, with steric repulsion only, adhesion only, and both effects simultaneously. The aspect ratio λ is varied according to the hd-protocol.

RNP diffusion under purely steric interactions has been discussed in the previous section. Under purely adhesive interactions, the RNP exhibits the non-monotonic behavior that Wang *et al.*[5] discovered. Short nanorods tend to be trapped by the attraction of a single adhesion site, while overly long ones can be captured and immobilized by simultaneous attraction of two adhesion sites. RNPs with an intermediate length comparable to the spacing between neighboring adhesion sites experience hopping diffusion at an elevated diffusivity. These observations align with the findings of Wang *et al.*[5] In particular, the maximum occurs at λ = 2, at which the RNP length is 209.6 nm, close to the nominal spacing r_0 = 200 nm between nearby adhesion sites.

To integrate both interactions into a single model, we adopt an approach different from that of Wang *et al.*[5] They first determined the diffusivity under steric repulsion and subsequently used it as the baseline onto which the adhesive interaction was added. When the two were integrated, neither was affected by the other, and the two interactions were not coupled directly.

In our BD simulation, on the other hand, both steric and adhesive interactions are realized in the geometry of a random fiber network. The two are directly coupled in the sense that if steric repulsion keeps an RNP away from a fiber, that may directly hinder their adhesion. We take this to be a more realistic representation. Indeed, the diffusivity of Fig. 10 reflects a direct competition between steric repulsion and adhesive attraction. D^t is higher than the purely adhesive case but lower than the purely steric case, indicating a balancing effect between the two interactions. The steric repulsion, which accounts for the finite thickness of the RNP, tends to shield the adhesive sites and elevates RNP diffusivity well above that for the case with pure adhesion. In particular, the tendency of longer rods being captured by two or more adhesion sites simultaneously is largely obviated by the steric shielding. As a result, D^t increases monotonically with λ; the local maximum observed under pure adhesion has been overpowered.

It will be interesting to examine the coupling between the two mechanisms more generally, for other types of attractive potential and a range of parameter values for U_0, ν and others, and perhaps for random distribution of adhesion sites on the polymer backbones. We leave such explorations to a separate endeavor.

4. Conclusions

In this work, we present Brownian dynamics simulations of rod-like nanoparticles (RNPs) diffusing in a random gel consisting of rigid fibers. Our observations show that in non-adhesive systems, RNP diffusivity increases monotonically with the RNP aspect ratio under the same hydrodynamic diameter. This trend is qualitatively similar to previous predictions of the obstruction-scaling (OS) model. Quantitatively, however,

Open Access Article. Published on 09 June 2025. Downloaded on 5/9/2026 5:04:01 AM.
This article is licensed under a Creative Commons Attribution-NonCommercial 3.0 Unported Licence.

our model predicts a diffusivity considerably higher than the OS model prediction.

We propose a new hypothesis to explain this discrepancy: a nanorod diffusing in a fibrous gel samples an effective pore-size distribution that differs from what the OS model assumes based on static geometry. We observe two modes of diffusion for RNPs in the networks: (a) the ''meandering diffusion'' occurs in coarser regions of the gel, characterized by lower translational diffusivity and higher rotational diffusivity; (b) the ''longitudinal diffusion'' occurs in denser regions, where tighter confinement by polymer chains limits RNP rotation and favors anisotropic diffusion along the long axis of the RNP, yielding lower rotational diffusivity and higher translational diffusivity. Moreover, the RNP spends considerably longer time in the meandering mode than the longitudinal mode. Effectively, therefore, the RNP samples preferably the coarser regions of the gel, and quickly traverses the denser regions by diffusing along its long axis. Both factors conspire to endow the long rods with superior diffusivity, much above what has previously been expected based on OS models. Our hypothesis has been supported by examining the average pore size in the gel surrounding either mode of diffusion, the number of close neighbors, and finally the anisotropic nature of the diffusion of rod-like NPs.

The above picture is counterintuitive, as one may expect NPs to linger in dense cages and to pass through coarse regions rapidly. The key to this puzzle is the anisotropic nature of the RNP diffusion, rooted in its shape anisotropy. Despite its great success for spherical NPs, the OS model turns out to be inaccurate for rod-like NPs. It estimates the obstruction by the polymer network solely from static geometry, disregarding the fact that in reality an NP has to trace out a continuous trajectory. In doing so, a rod-like NP experiences the hydrogel in a dynamic way that differs considerably from expectations based on the static geometry. We further assessed the discrepancy between the OS model predictions and our BD results by using experimental data. Our model shows better agreement with data than the extended OS model.

Furthermore, we have explored the interplay between steric and adhesive interactions. We demonstrate that it is essential to directly couple the two mechanisms, and that steric repulsion can shield certain adhesive sites, thereby diminishing the overall adhesion forces experienced by the RNP and resulting in a diffusivity that is intermediate between the purely steric and purely adhesive cases.

In examining the movement of the RNP through the network of rigid fibers, one may note a potential connection to reptation models for entangled polymers,[37,38] and in particular the Doi theory for rod-like polymers.[39] In a sense, the diffusive motion of the RNP in our context parallels that of a polymer reptating through a tube formed by entangled neighboring polymer chains; see Fig. 9.3 of Doi & Edwards.[38] But there is a key difference, which is essentially the difference between a liquid and a gel. In the reptation models, the tube itself is constantly remodeling, thus giving rise to the flowability and viscoelasticity of the polymeric liquid. In the gel models, either with flexible polymers[14] or rigid ones (our model), the polymer chains are cross-linked ''permanently'', at least until yielding, and the medium remains an elastic solid permeated with liquid solvent.

We must point out a few simplifications in our model. First, we have neglected the flexibility of the polymer network. If the polymer chains can fluctuate and deform, they would allow the RNP more freedom in its diffusion, potentially increasing its diffusivity.[6,14] To remedy this shortcoming, we may extend our description of the polymer network as composed of bead-spring chains, following earlier molecular dynamics models.[6,14] Second, we have disregarded the hydrodynamic interaction (HI) between the RNP and the polymer chains. This could potentially increase the drag on the RNPs and reduce their diffusivity, especially when the RNP size is not much smaller than the pore size. Historically, HI has been accounted for *via* friction tensors originally developed for rigid spherical particles,[23] and has been generalized to bead-spring models for polymer chains.[24] This points to a method of adding HI to our RNP diffusion problem. Granted, the degree of complexity and magnitude of computation will be greatly augmented. Third, the spatial distribution of adhesion sites in real gels can differ from the roughly uniform distribution assumed in our model. Such spatial fluctuations may modify the long-time RNP diffusivity even if the overall density of adhesion sites is kept unchanged. Besides, we have not explored the effect of changing that density. Finally, polymeric fibers in real systems possess a finite thickness. Although our model is capable of accounting for finite-sized fibers, we performed all simulations with zero-thickness fibers in order to closely mimic the theoretical study of Wang *et al.*[5] Incorporating finite fiber thickness would likely lead to reduced diffusivity, due to enhanced steric repulsion between the fibers and the diffusing particles. In light of the above limitations, our model should be viewed as a starting point for modeling diffusion of RNPs in realistic biological gels.

Thus, our Brownian model lays the groundwork for future extensions, *e.g.*, to incorporate HI and network deformation. In spite of the above limitations, our simulations have provided deeper insights into the diffusion of rod-like nanoparticles in hydrogels, uncovering the role of anisotropic diffusion that can greatly boost the translational diffusivity of RNPs. Our findings can be leveraged to guide the design of nanoparticles optimized for targeted drug delivery through biopolymer gels like mucus.

Data availability

The computational methods for generating the numerical results, including the temporal discretization scheme, the statistical analysis of data and parameter evaluation, are described in the ESI.† The numerical code is available online: **https://github.com/mrokhfrooz/BD_simulation_rodlike_nanoparticle_gels**.

Conflicts of interest

There are no conflicts to declare.

Open Access Article. Published on 09 June 2025. Downloaded on 5/9/2026 5:04:01 AM. This article is licensed under a Creative Commons Attribution-NonCommercial 3.0 Unported Licence.

Acknowledgements

The authors gratefully acknowledge financial support from Mitacs Canada and Providence Healthcare (IT19059) and from the Natural Sciences and Engineering Research Council of Canada (Discovery Grant No. 2019-04162, 2024-03982 and Alliance International Grant No. 586462-23). They also extend their thanks to Joerg Rottler, Simcha Srebnik, Belal Tafech, and Jiuling Wang for fruitful discussions. This research was supported in part through the computational resources and services provided by Advanced Research Computing at the University of British Columbia.

References

1 D. Li, X. Li, J. Bai, Y. Liu, R. de Vries and Y. Li, *Int. J. Biol. Macromol.*, 2021, **166**, 401–408.
2 B. Tafech, M. R. Rokhforouz, J. Leung, M. M. H. Sung, P. J. C. Lin, D. D. Sin, D. Lauster, S. Block, B. S. Quon, Y. Tam, P. Cullis, J. J. Feng and S. Hedtrich, *Adv. Healthcare Mater.*, 2024, **13**, 2304525.
3 N. Zheng, J. Li, C. Xu, L. Xu, S. Li and L. Xu, *Artif. Cells, Nanomed., Biotechnol.*, 2018, **46**, 1132–1140.
4 M. Yu, J. Wang, Y. Yang, C. Zhu, Q. Su, S. Guo, J. Sun, Y. Gan, X. Shi and H. Gao, *Nano Lett.*, 2016, **16**, 7176–7182.
5 J. Wang, Y. Yang, M. Yu, G. Hu, Y. Gan, H. Gao and X. Shi, *J. Mech. Phys. Solids*, 2018, **112**, 431–457.
6 C. Bao, B. Liu, B. Li, J. Chai, L. Zhang, L. Jiao, D. Li, Z. Yu, F. Ren and X. Shi, *Nano Lett.*, 2020, **20**, 1352–1361.
7 M. Guo, M. Wei, W. Li, M. Guo, C. Guo, M. Ma, Y. Wang, Z. Yang, M. Li and Q. Fu, *J. Controlled Release*, 2019, **307**, 64–75.
8 K. A. Rose, N. Gogotsi, J. H. Galarraga, J. A. Burdick, C. B. Murray, D. Lee and R. J. Composto, *Macromolecules*, 2022, **55**, 8514–8523.
9 A. Banerjee, J. Qi, R. Gogoi, J. Wong and S. Mitragotri, *J. Controlled Release*, 2016, **238**, 176–185.
10 W. Liu, L. Zhang, Z. Dong, K. Liu, H. He, Y. Lu, W. Wu and J. Qi, *Nano Res.*, 2022, **15**, 9243–9252.
11 B. Xue, Y. Liu, Y. Tian and P. Yin, *Nat. Commun.*, 2024, **15**, 6502.
12 X. Zhang, X. Dai, M. A. Habib, L. Gao, W. Chen, W. Wei, Z. Tang, X. Qi, X. Gong and L. Jiang, *Nat. Commun.*, 2024, **15**, 525.
13 J. Wang and X. Shi, *Acta Mech. Solida Sin.*, 2017, **30**, 241–247.
14 B.-R. Zhao, B. Li and X. Shi, *Nanoscale*, 2021, **13**, 17404–17416.
15 S.-J. Li, H.-J. Qian and Z.-Y. Lu, *Phys. Chem. Chem. Phys.*, 2018, **20**, 20996–21007.
16 J. Wang, T. C. O'Connor, G. S. Grest, Y. Zheng, M. Rubinstein and T. Ge, *Macromolecules*, 2021, **54**, 7051–7059.
17 A. G. Ogston, *Trans. Faraday Soc.*, 1958, **54**, 1754–1757.
18 J. Hansing, C. Ciemer, W. K. Kim, X. Zhang, J. E. DeRouchey and R. R. Netz, *Eur. Phys. J. E:Soft Matter Biol. Phys.*, 2016, **39**, 1–13.
19 R. A. Cone, *Adv. Drug Delivery Rev.*, 2009, **61**, 75–85.
20 J. C. Berg, *An introduction to interfaces and colloids: the bridge to nanoscience*, World Scientific, 2010.
21 A. Ortega and J. Garcıa de la Torre, *J. Chem. Phys.*, 2003, **119**, 9914–9919.
22 A. Saadat and B. Khomami, *J. Rheol.*, 2017, **61**, 147–149.
23 D. L. Ermak and J. A. McCammon, *J. Chem. Phys.*, 1978, **69**, 1352–1360.
24 C.-C. Hsieh, L. Li and R. G. Larson, *J. Non-Newtonian Fluid Mech.*, 2003, **113**, 147–191.
25 A. Satoh, *Modeling of magnetic particle suspensions for simulations*, CRC Press, 2017.
26 H. Löwen, *Phys. Rev. E:Stat. Phys., Plasmas, Fluids, Relat. Interdiscip. Top.*, 1994, **50**, 1232.
27 M. M. Tirado, C. L. Martínez and J. G. De La Torre, *J. Chem. Phys.*, 1984, **81**, 2047–2052.
28 T. Kirchhoff, H. Löwen and R. Klein, *Phys. Rev. E:Stat. Phys., Plasmas, Fluids, Relat. Interdiscip. Top.*, 1996, **53**, 5011.
29 J.-Y. Chen, Z. Li, I. Szlufarska and D. J. Klingenberg, *J. Rheol.*, 2021, **65**, 273–288.
30 M. T. Klann, A. Lapin and M. Reuss, *Biophys. J.*, 2009, **96**, 5122–5129.
31 M. Quesada-Pérez and A. Martín-Molina, *Adv. Colloid Interface Sci.*, 2021, **287**, 102320.
32 T. Stylianopoulos, B. Diop-Frimpong, L. L. Munn and R. K. Jain, *Biophys. J.*, 2010, **99**, 3119–3128.
33 D. Arcizet, B. Meier, E. Sackmann, J. O. Rädler and D. Heinrich, *Phys. Rev. Lett.*, 2008, **101**, 248103.
34 X. He, Y. Yang, Y. Han, C. Cao, Z. Zhang, L. Li, C. Xiao, H. Guo, L. Wang and L. Han, *Proc. Natl. Acad. Sci. U. S. A.*, 2023, **120**, e2209260120.
35 N. Arfin and H. B. Bohidar, *Int. J. Biol. Macromol.*, 2012, **50**, 759–767.
36 M. Yu, L. Xu, F. Tian, Q. Su, N. Zheng, Y. Yang, J. Wang, A. Wang, C. Zhu and S. Guo, *Nat. Commun.*, 2018, **9**, 2607.
37 P.-G. De Gennes, *J. Chem. Phys.*, 1971, **55**, 572–579.
38 M. Doi, S. F. Edwards and S. F. Edwards, *The theory of polymer dynamics*, Oxford University Press, 1988, vol. 73.
39 M. Doi, *J. Polym. Sci., Polym. Phys. Ed.*, 1981, **19**, 229–243.